Experimental Thermal and Fluid Science 40 (2012) 93–102

Contents lists available at SciVerse ScienceDirect

Experimental Thermal and Fluid Science

journal homepage: www.elsevier.com/locate/etfs

Copper foam based vapor chamber for high heat flux dissipation

Xianbing Ji [a], Jinliang Xu [a,b,*], Aime Marthial Abanda [c]

[a] State Key Laboratory of Alternate Electrical Power System with Renewable Energy Sources, North China Electric Power University, Beijing 102206, PR China
[b] The Beijing Key Laboratory of New and Renewable Energy, North China Electric Power University, Beijing 102206, PR China
[c] The Beijing Key Laboratory of Multiphase Flow and Heat Transfer, North China Electric Power University, Beijing 102206, PR China

ARTICLE INFO

Article history:
Received 30 July 2011
Received in revised form 27 January 2012
Accepted 11 February 2012
Available online 3 March 2012

Keywords:
Copper foam
Capillary wick
Vapor chamber
Heat transfer

ABSTRACT

A copper foam based vapor chamber was designed, built and tested in this paper. The vapor chamber consists of a top and bottom copper foam pieces which are sintered on the two copper plates. Several copper foam bars directly contact the tip of the condenser and evaporator wicks. The surface temperature non-uniformity was defined to characterize the temperature distribution on the condenser and evaporator surfaces. It is found that the water and ethanol based vapor chambers have the best and worst thermal performance, respectively, among the three working fluids of water, acetone and ethanol. The surface temperature non-uniformity on the bottom (evaporator) surface are 3–5 times of those on the top (condenser) surface. Generally thermal resistances of vapor chambers are decreased with increases in heating powers. Charge ratios and inclined angles are combined to influence the thermal performance of vapor chambers. The maximum heating power attains 170 W, corresponding to the heat flux of 216 W/cm^2 without the capillary or boiling limits reached. The minimum thermal resistance is 0.09 K/W. The significantly extended operation range of heat flux is due to the distinct nature of high porosity and multiscale pore sizes of copper foams.

1. Introduction

Miniaturization of electronic devices such as LED (light emitting diodes) and computer chips leads to high heat flux to be dissipated. As an effective flat plate heat pipe, a vapor chamber has a uniform temperature distribution. A vapor chamber is a two-phase heat transfer device. The inner wick on the bottom wall in contact with the electronic chips serves as the evaporator, where the liquid evaporates and carries heat away from the heating surface. The upper wall functions as the condenser where the vapor condenses and releases the latent heat, which is dissipated out through the adjacent fin heat sink. The condensed liquid is recycled back to the evaporator by capillary force.

The capillary wick in a vapor chamber pumps liquid to the heating surface. There are three kinds of capillary wicks in the literature: (1) the sintered powder wick provides large capillary force, but large shear stress occurs during the counter-current flow of vapor and liquid phases in porous pores; (2) the mesh wick can control the thermal resistance by adjusting the combination degree between wires. The shortcoming of the mesh wick is the large temperature drop in the thickness direction of the mesh wick; (3) the microchannel structure significantly decreases the shear stress at the vapor–liquid interface during the counter-current flow of the two phases, yielding the enhanced heat transfer.

Wang and Vafai [1,2] studied the thermal performance of a flat plate heat pipe, showing quite uniform temperatures along the heat pipe wall surfaces. They indicate that the porous wick of the evaporator section creates the main thermal resistance to yield the largest temperature drop, consequently affecting the heat pipe performance.

Wang and Peterson [3] proposed a novel flat plate heat pipe design. Sintered copper screen mesh was used as the primary wick structure, in conjunction with a series of parallel wires, which formed liquid arteries. Water was used as the working fluid. The maximum heat transport capacity was examined and the design parameters of this particular design were optimized.

Cao and Gao [4] fabricated miniature heat pipes using the electric-discharge-machining (EDM) wire-cutting method. Axial grooves can be created around the entire interior perimeters of the miniature heat pipes. The effective thermal conductance of the heat pipe is on the order of 40 times that of copper based on the external cross-sectional area of the miniature heat pipe.

Hophins et al. [5] investigated the maximum heat transfer capabilities of two copper–water flat miniature heat pipes (FMHP) with diagonal trapezoidal micro capillary grooves and one copper–water FMHP with axial rectangular micro capillary grooves. Maximum heat flux on the evaporator wall of the 120 mm long axial grooved heat pipe, with a vapor channel cross-sectional area of approximately 1.5×12 mm^2 and rectangular grooves of dimensions

* Corresponding author at: The Beijing Key Laboratory of New and Renewable Energy, North China Electric Power University, Beijing 102206, PR China. Tel./fax: +86 10 61772268.
E-mail address: xjl@ncepu.edu.cn (J. Xu).

0894-1777/$ - see front matter © 2012 Elsevier Inc. All rights reserved.
doi:10.1016/j.expthermflusci.2012.02.004

Nomenclature

A_e	wick surface area of the evaporator (m^2)
A_l	cross-sectional area of the wick perpendicular to the liquid flow direction (m^2)
a_0 and a_1	empirically determined constants for temperature distribution in copper block
b	charge ratio
d_f	ligament diameter of metallic foam, m
d_p	pore diameter of metallic foam, m
d_{eff}	effective pore diameter of the wick, m
G	combined parameter for the porous wick, $G = \frac{A_l \varepsilon_p^2 \cos\alpha}{A_e \Delta x d_{eff}}$
h_{lg}	latent heat of evaporation (J/kg)
K	permeability (m^2)
k	thermal conductivity of copper (W/(m K))
l	ligament length of a unit cell of metallic foams, m
N	combined parameter for working liquid, $N = \frac{\sigma \rho_l h_{lg}}{\mu_l}$ (W/m^2)
p	pressure (Pa)
ppi	number of pores per inch
q	heat flux (W/m^2)
q'	evaporator heat flux (W/m^2)
Q	effective heating power (J)
R	thermal resistance (K/W)
T	temperature (K or °C)
r	cylindrical coordinate (m)
U	surface temperature non-uniformity (K/W)
u	liquid surface velocity (m/s)
z	axial coordinate (m)
$\frac{dT}{dz}\|_J$	temperature gradient at the junction location (K/m)
Δp	pressure drop (Pa)
Δx	distance for the liquid flow path (m)

Greek symbols

α	wetting angle
ε	porosity
σ	liquid surface tension (N/m)
μ	viscosity (kg/(m s))
ρ	density (kg/m^3)

Subscripts

ave	average
bot	bottom surface
c	capillary
eff	effective
g	gravity
J	junction between vapor chamber and heating copper block
l	liquid
max	maximum
min	minimum
s	solid
sat	saturation condition
top	top surface
v	vapor phase
VC	vapor chamber

0.20 mm wide by 0.42 mm deep, exceeded 90 W/cm^2 in the horizontal orientation and 150 W/cm^2 in the vertical orientation.

Vasiliev [6] pointed out that the micro grooved flat plate heat pipes have large heat transfer coefficients and heat transfer area for the fluid per unit volume. They compared the sintered powder wick, micro grooved capillary wick, and screen mesh wick structures used in flat plate heat pipes. They concluded that the sintered powder wick is the most effective, and optimization of the sintered powder parameters is important to improve the thermal performance of flat plate heat pipes.

Lu et al. [7] tested a vapor chamber using high thermal conductivity and permeability graphite foam as the wick structure. The vapor chamber can reach a heat flux of 80 W/cm^2 with ethanol as the working fluid. Effects of the capillary limit, boiling limit, and thermal resistance in restricting the overall performance of a vapor chamber were analyzed. Their modeling results show that the vapor chamber performance using graphite foam is about twice that of one using a copper powder wick structure.

Wong et al. [8] invented a novel vapor chamber and studied its performance. Parallel grooves are made on the inner surface of the top plate, with inter-groove openings, to replace the conventional porous wick. The inner surface of the bottom plate is sintered a layer of porous wick as the evaporator. The peaks of the groove walls directly contact with the wick so that the grooves function as vapor path, condenser and structural supporters simultaneously. Good performances with low vapor chamber resistance and large heat load limit were obtained under different orientations.

Metallic foam is a new kind of heat transfer material that has been received great attention in recent years. It behaves large thermal conductivity and ultra light. Besides, it has large porosity such as 0.95 used in this study. Single-phase liquid/gas heat transfer in confined channels and boiling heat transfer under pool or forced convection conditions have been reported in the literature. However, there are no reports on the metallic foam based vapor chambers in the open literature, to the authors' knowledge.

The motivation of the present study is to pursue the possibility that metallic foam can be used as the capillary wick in vapor chambers for high heat flux dissipation. The vapor chamber consists of a top and bottom copper foam pieces which are sintered on the two copper plates. Several copper foam bars directly contact the tip of the condenser and evaporator wicks. Three working fluids of water, acetone and ethanol are tested. Charge ratios are changed from 0.15 to 0.45, and inclination angles are from horizontal to vertical orientations. A new parameter, i.e. the surface thermal resistance was defined to characterize the temperature uniformity on the condenser and evaporator surfaces. Effects of working fluids, charge ratios and inclination angles on the thermal performance of vapor chambers were discussed and analyzed. The capillary limit or boiling limit was not reached at the heating power of 170 W, corresponding to the heat flux of 216 W/cm^2, which is significantly larger than those reported in the references.

2. The test section and experimental setup

2.1. Design of the copper foam based vapor chamber

Fig. 1a shows the piece components which can be combined to form a vapor chamber, consisting of top copper cap (1), copper foam piece (2), copper foam bar (3), copper foam piece (4), miniature copper cylinder (5), copper foam skirt (6), and copper substrate (7). The grey and red colors represent the copper material and copper foam material, respectively (see Fig. 1a). The copper foam piece (2) was sintered on the inner surface of the top copper cap (1), and the copper foam piece (4) was sintered on the inner surface of the copper substrate (7). The top and bottom copper plates were welded together to form the vapor chamber. The four miniature copper cylinders (5) support the whole vapor chamber

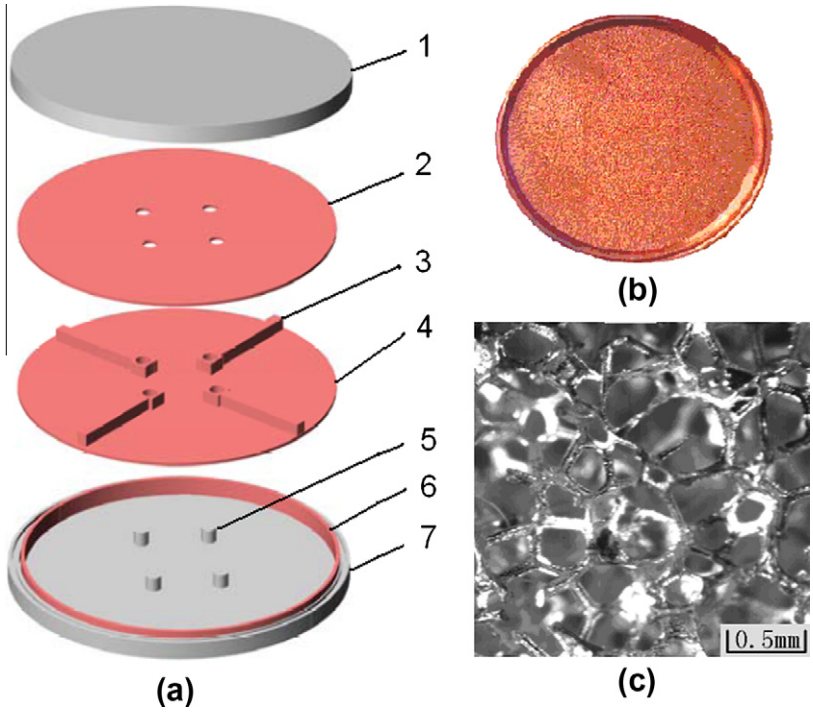

Fig. 1. The vapor chamber structure (a) pieces for vapor chamber, (b) photo of the copper foam sintered on the evaporator surface, (c) photo of the copper foam (1: top copper cap, 2: copper foam piece, 3: copper foam bar, 4: copper foam piece, 5: miniature copper cylinder, 6: copper foam skirt, 7: copper substrate, the gray color indicates the copper material and the red color represents the copper foam material in Fig. 1a). (For interpretation of the references to color in this figure legend, the reader is referred to the web version of this article.)

to prevent the structure deformation during the vacuum process of the vapor chamber. The foam bars (3) directly contact the tip of the top and bottom foam pieces. In conventional vapor chamber, liquid is returned from the chamber side wall to the heater location. However, the copper foam bars significantly decrease the liquid flow path, helping to recycle the liquid from the condenser to the evaporator wick.

Fig. 1b shows the photo of the copper foam sintered on the inner copper substrate surface. The copper foam has a porosity of 0.95 and ppi of 90 (see Fig. 1c). The foam has an open-celled structure, having 12–14 pentagonal or hexagonal faces. The cross-section of ligaments depends on porosity, and changes from a circle at $\varepsilon = 0.85$ to an inner concave at $\varepsilon = 0.97$ ([9]) Fig. 2 shows a unit foam cell, with the assumed tetrakaidecahedron shape. The ligament length is l with its diameter of d_f. The circumcircle diameter of the foam cell is $\sqrt{10}l$, which can be regarded as the pore diameter of d_p, i.e. $d_p = \sqrt{10}l$ (not considering the ligament thickness). In the present study, the pore diameter of d_p equals to 0.772 mm. We visualized the minimum pore diameter as 0.09 mm, which is also regarded as the effective pore diameter of d_{eff} to affect the liquid suction. Coexistence of large and small pores in foams is helpful for the vapor release from the large pores and liquid suction in small pores, improving the vapor chamber performance. The ligament length l and diameter d_f are 0.299 mm and 0.064 mm, respectively.

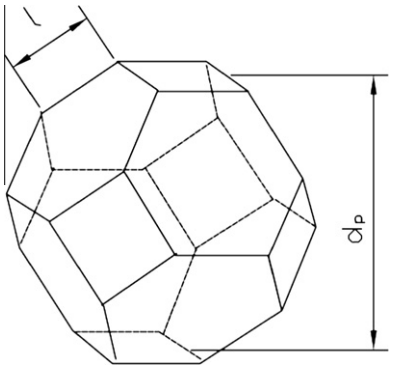

Fig. 2. A unit of foam structure.

2.2. The vapor chamber assembly for experiment

The vapor chamber and the heating copper block was welded together to form the vapor chamber assembly, thus there is no any contact thermal resistance between them (see Fig. 3). The vapor chamber has a diameter of 100 mm and a thickness of 8.0 mm. The wall thickness of the vapor chamber is 1.2 mm. Both the two copper foam pieces sintered on the inner surface of the vapor chamber have the thickness of 2.0 mm. There is a capillary tube connected with the side wall of the vapor chamber, acting as the vacuum port and liquid charge port. Before charging liquid into the vapor chamber, the vapor chamber was vacuumed to a pressure of 6×10^{-3} Pa. After the vapor chamber was charged with liquid, the pressure in the vapor chamber consists of the pressure due to the non-condensable gas and the vapor–liquid phase equilibrium pressure. The later component depends on the charged liquid and the environment temperature. For example, the phase equilibrium pressure for ethanol is 7.83 k Pa at the environment temperature of 25 °C, which is three orders higher than the non-condensable gas pressure. Thus the non-condensable gas pressure has less influence on the vapor chamber performance.

The heating copper block was machined with the bottom part as a prism, the central part as a pyramid, and the top part as a cylinder, ensuring uniform heat conduction in the cylinder part along the axial direction. The 10 mm diameter cylinder was welded on the vapor chamber surface centrally. Totally 18 K-type

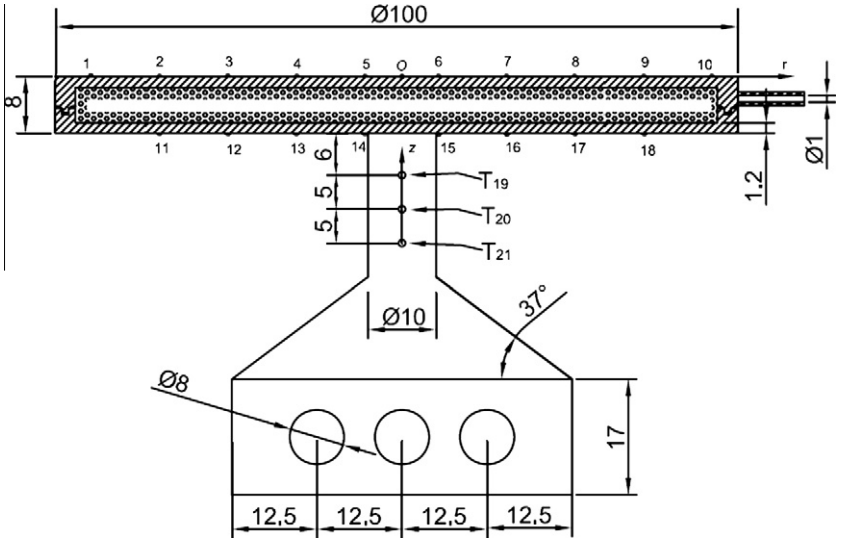

Fig. 3. The assembly of vapor chamber and heating copper block.

thermocouples were welded on the top and bottom surfaces of the vapor chamber. They are numbered from 1 to 10 on the top surface, and from 11 to 18 on the bottom surface. The distance between two neighboring thermocouples is 10 mm. In order to accurately evaluate the heat flux and temperature at the junction between the heating cylinder and the vapor chamber surface, three thermocouple wires, which are numbered from 19 to 21 in Fig. 3, are inserted in 1 mm diameter holes of the cylinder. Then the holes are filled with glue having a 200 °C temperature tolerance and 58.7 W/m K thermal conductivity.

2.3. The experimental setup

Fig. 4a shows the experimental setup. The vapor chamber assembly was attached on the base surface of a fin heat sink, with glue filled between them. The fin heat sink has exactly the same diameter of 100 mm as that of the vapor chamber. There are totally 23 fins, each having a thickness of 2.0 mm and height of 53 mm. The gap between two neighboring fins is 2.5 mm. There is a cooling fan arranged at the top of the fin heat sink. Fig. 4b shows the thermocouple arrangement on the top surface of the vapor chamber. For each thermocouple wire, there is a 1 mm-diameter hole on the fin base, from which the thermocouple wire can be penetrated to the hardware external.

Three cartridge heaters were used, each having a maximum heating power of 100 W at the AC voltage of 220 V. The three cartridge heaters are driven by a power supply system, consisting of a voltage stabilizer, an AC voltage transformer and a power-meter. The voltage stabilizer significantly minimized the voltage oscillation versus time. By adjusting the voltage transformer, one can obtain a stable voltage output in the range of 2–220 V, resulting in controlled adjustable heating power up to 300 W.

Before the welding process of the vapor chamber, all the pieces were rinsed by methanol liquid. The vacuum and charging procedures were performed using a special facility fabricated in our laboratory. The vapor chamber was filled with the working fluid and sealed. The final net liquid charged in the vapor chamber was the weight difference before and after the vapor chamber was charged with liquid. Such weight measurement was performed by an electronic balance with the accuracy of 0.01 g. The total inside volume of the vapor chamber was 34.5 ml. The charge ratio (b) is defined as the liquid volume occupied by the total inside volume of the vapor chamber. The charge ratio is estimated to have an uncertainty of 0.5%.

2.4. Data reduction and uncertainty analysis

It is noted that the cooper block under the vapor chamber is wrapped by the insulation material. Heat flux can be determined at the junction surface between the vapor chamber and the copper block, which can be written as $q = -k\frac{dT}{dz}|_J$ based on the one-dimensional assumption, where k is the temperature dependent thermal conductivity of copper, $\frac{dT}{dz}|_J$ is the temperature gradient at the junction location, z is the coordinate perpendicular to the junction surface (see Fig. 3). A least square correlation of temperatures versus z was written as $T = a_0 + a_1 z$, where a_0 and a_1 are the constants correlated based on T_{19}, T_{20} and T_{21} (see Fig. 3). The junction temperature (T_J) is the maximum temperature at the bottom vapor chamber surface and can also be decided in terms of such correlation. The calculated heating power is about 92% of that measured by the power meter. In order words, the heat loss is about 8%. The difference between T_j by the liner curve correlation with T_{14} and T_{15} is increased with increases in the heating powers. For example, T_j deviates from T_{14} and T_{15} by 2.7 °C at $Q = 100$ W, and deviates from T_{14} and T_{15} by 3.6 °C at $Q = 150$ W.

It is necessary to evaluate the thermal resistance of the vapor chamber, which is defined as

$$R_{VC} = \frac{T_j - T_{ave,top}}{Q} \tag{1}$$

where $T_{ave,top}$ is the average temperature at the top condenser surface of the vapor chamber, which is expressed as (see Fig. 3)

$$T_{ave,top} = \frac{\sum_{i=1}^{10} T_i}{10} \tag{2}$$

In order to characterize the uniformity of the temperature distribution on the top and bottom surfaces of the vapor chamber, we define the new parameters of surface temperature non-uniformity, which are expressed as

$$U_{s,top} = \frac{T_{max,top} - T_{min,top}}{Q} \tag{3}$$

$$U_{s,bot} = \frac{T_{max,bot} - T_{min,bot}}{Q} \tag{4}$$

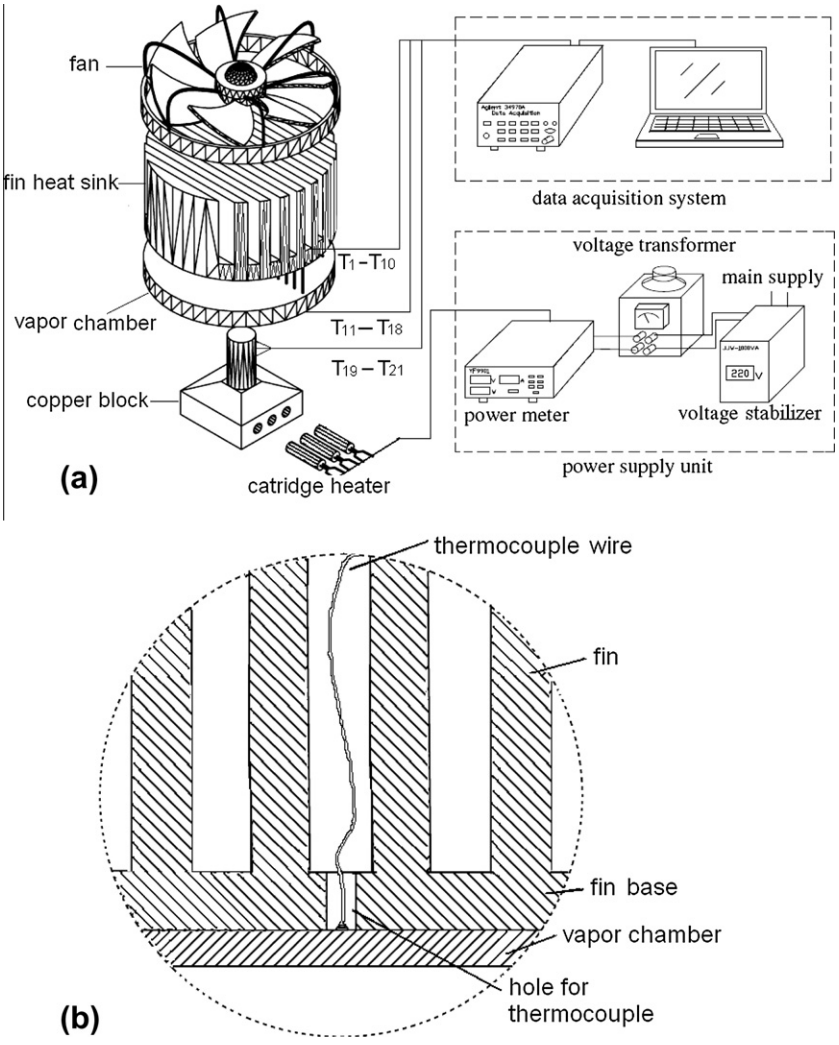

Fig. 4. The experimental setup.

where $U_{s,top}$ and $U_{s,bot}$ are the surface temperature non-uniformity at the top and bottom surfaces of the vapor chamber, respectively, $T_{max,top} = \max(T_1–T_{10})$, $T_{min,top} = \min(T_1–T_{10})$, $T_{max,bot} = \max(T_{11}–T_{18})$, $T_{min,bot} = \min(T_{11}–T_{18})$, see Fig. 3. Physical meaning of the surface temperature non-uniformity is the maximum temperature difference per unit heating power. Heat flux q is defined as the heating power divided by the junction heater area.

The temperature measurements involve the maximum uncertainty of 0.2 K. The power-meter gave an accuracy of 0.5% for the heating power. The thermal resistance for the vapor chamber depends on the temperature and heating power measurements. The standard uncertainty analysis gives

$$\Delta R_{VC} = \sqrt{\left(\frac{\partial R_{VC}}{\partial T_J}\right)^2 \Delta T_J^2 + \left(\frac{\partial R_{VC}}{\partial T_{ave,top}}\right)^2 \Delta T_{ave,top}^2 + \left(\frac{\partial R_{VC}}{\partial Q}\right)^2 \Delta Q^2} \quad (5)$$

Substituting the expression of the thermal resistance defined in Eq. (1) into Eq. (5), we have the relative error for the thermal resistance as

$$\frac{\Delta R_{Vc}}{R_{Vc}} = \sqrt{\left(\frac{\Delta Q}{Q}\right)^2 + \left(\frac{\Delta T_J}{T_J - T_{ave,top}}\right)^2 + \left(\frac{\Delta T_{ave,top}}{T_J - T_{ave,top}}\right)^2} \quad (6)$$

Eq. (6) gave the uncertainty of 6.1% for the thermal resistance of the vapor chamber. Similarly, the standard uncertainty analysis gave the uncertainties of 10.5% and 6.3% for the surface temperature non-uniformity on the top and bottom vapor chamber surfaces.

3. Results and discussion

3.1. Analysis of vapor chamber performance

For the steady operation of a vapor chamber, the capillary pressure (Δp_c) created by the wick structure is the driven source for the fluid circulation in the closed volume. Δp_c should be larger or equal to the sum of the liquid pressure drop (Δp_l), vapor pressure drop (Δp_v), and gravity induced pressure drop (Δp_g), i.e.

$$\Delta p_c \geq \Delta p_l + \Delta p_v + \Delta p_g \quad (7)$$

where Δp_c is

$$\Delta p_c = \frac{4\sigma \cos\alpha}{d_{eff}} \quad (8)$$

where σ is the surface tension of liquid, α is the wetting angle, d_{eff} is the effective pore diameter of the wick, which is dependent on the minimum pore diameter of the metallic foam.

Because the liquid flow velocity and pore diameter are very small, Reynolds number for the liquid flow is very small and the flow is in laminar flow region. The pressure drop for the liquid flow can be estimated in terms of the Darcy's equation:

$$\Delta p_l = \frac{\mu_l u_l}{K} \Delta x \quad (9)$$

where μ_l is the liquid viscosity, u_l is the liquid surface velocity, K is the porous permeability, which can be expressed as

$$K = \frac{\varepsilon d_p^2}{32} \tag{10}$$

and Δx is the distance for the liquid flow path. In this study, the copper foam bar directly contacts the evaporator and condenser surface, greatly decreasing the flow path for the liquid flow.

The following energy equation gives the relationship between the evaporator heat flux and required liquid flow

$$q' A_e = \rho_1 \mu_1 A_1 h_{lg} \tag{11}$$

where q' is the evaporator heat flux, A_e is the wick surface area of the evaporator, ρ_l is the liquid density, A_l is the cross-sectional area of the wick perpendicular to the liquid flow direction, which is filled with liquid, h_{lg} is the latent heat of evaporation. The evaporator heat flux can be reached based on Eqs. (8)–(11), by neglecting the vapor pressure drop and gravity pressure drop:

$$q' = \frac{1}{8} NG \tag{12}$$

where $N = \frac{\sigma \rho_l h_{lg}}{\mu_l}$ is completely dependent on the working fluid and $G = \frac{A_l \varepsilon d_p^2 \cos\alpha}{A_e \Delta x d_{eff}}$ is a combined parameter for the porous wick. It is seen from the G parameter that a good vapor chamber performance can be obtained using a large pore diameter d_p, a low wetting angle α, and a small effective porous diameter d_{eff}. Metallic foam behaves such characteristics, thus it is an ideal porous media material used in vapor chambers. Fig. 5 shows the surface tension, viscosity, and N number versus liquid temperature. Among the three working fluids of water, acetone and ethanol, water has the largest N number, which is about 12–17 times of acetone and ethanol. It would be expected that the water based vapor chamber has the best thermal performance.

3.2. The surface temperature non-uniformity

Fig. 6 shows the surface temperature distribution for the liquid charged vapor chamber, empty (non-liquid filled) vapor chamber, and copper plate. The copper plate has exactly the same overall size and material as those of the vapor chamber. As shown in Fig. 6a–b, very uniform temperature distribution can be seen at the condenser surface of the liquid filled vapor chamber, i.e. top surface (referring to T_1–T_{10} in Fig. 3). The maximum temperature difference on the condenser surface is only 1.1 °C at the heating load of 150 W. On the bottom surface of the vapor chamber, temperatures (T_{11}–T_{18} in Fig. 3) are larger at the center area and are decreased with increases in the r coordinate (away from the center area). For the copper plate, however, significant non-uniform temperature distribution is identified, especially at the bottom surface of the copper plate. For instance, the copper plate has a temperature of 91 °C at the location having 5 mm distance away from the center of heating area for the heating power of 150 W. But the vapor chamber has only the temperature of 71 °C at the same location and heating power (see Fig. 6b). Generally, the center location has higher temperatures than the side locations for the copper plate.

The non-uniformity of the surface temperatures is greater for the empty vapor chamber than the liquid charged vapor chamber and copper plate. The empty vapor chamber has lower temperatures at the center area than that at the side area on the top surface (see Fig. 6c), due to the heat conduction from the side wall to the center area. The bottom surface of the empty vapor chamber has much higher temperatures than the liquid charged vapor chamber (see Fig. 6d). For instance, the center area of the empty vapor chamber has a temperature of 102 °C, but the liquid charged vapor chamber has the temperature of 77 °C at Q = 90 W.

The surface temperature non-uniformity give the temperature uniformity information on the two surfaces for the vapor chamber. Fig. 7a and b shows the surface temperature non-uniformity dependent on the working fluids at the horizontal orientation ($\theta = 0°$) and charge ratio of 0.30. The empty vapor chamber has significantly large surface temperature non-uniformity on both surfaces than the copper plate and liquid charged vapor chamber. Both the empty vapor chamber and copper plate have nearly constant surface temperature non-uniformity, due to the heat conduction mechanism. Among the three working fluids of water, acetone and ethanol, the water and ethanol charged vapor chamber have the smallest and largest surface temperature non-uniformity, respectively. Effect of working fluids on the surface temperature non-uniformity is consistent with the N number analysis, i.e. water has the largest N number to have best thermal performance. For all

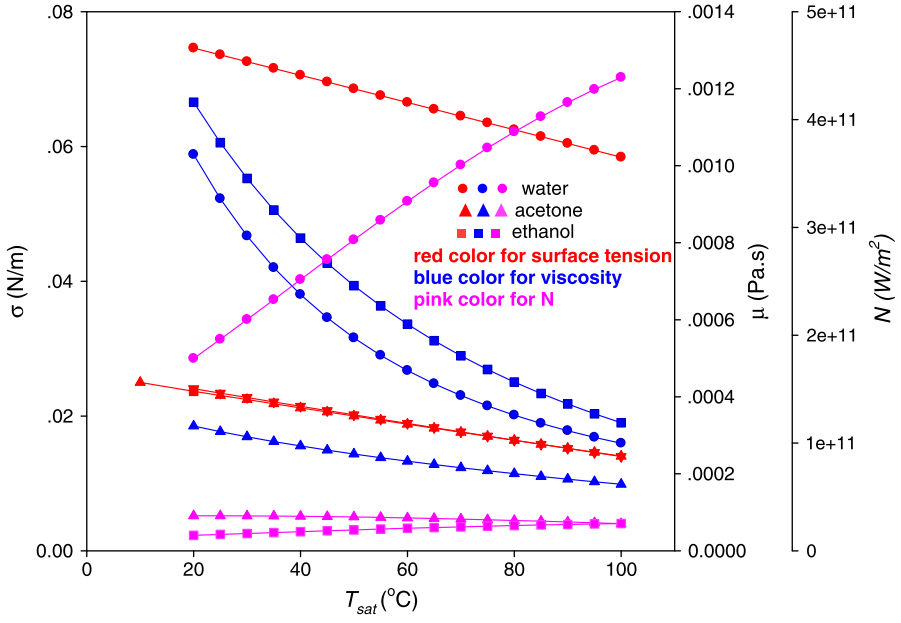

Fig. 5. The surface tension, viscosity and N number versus saturation temperature for water, acetone and ethanol.

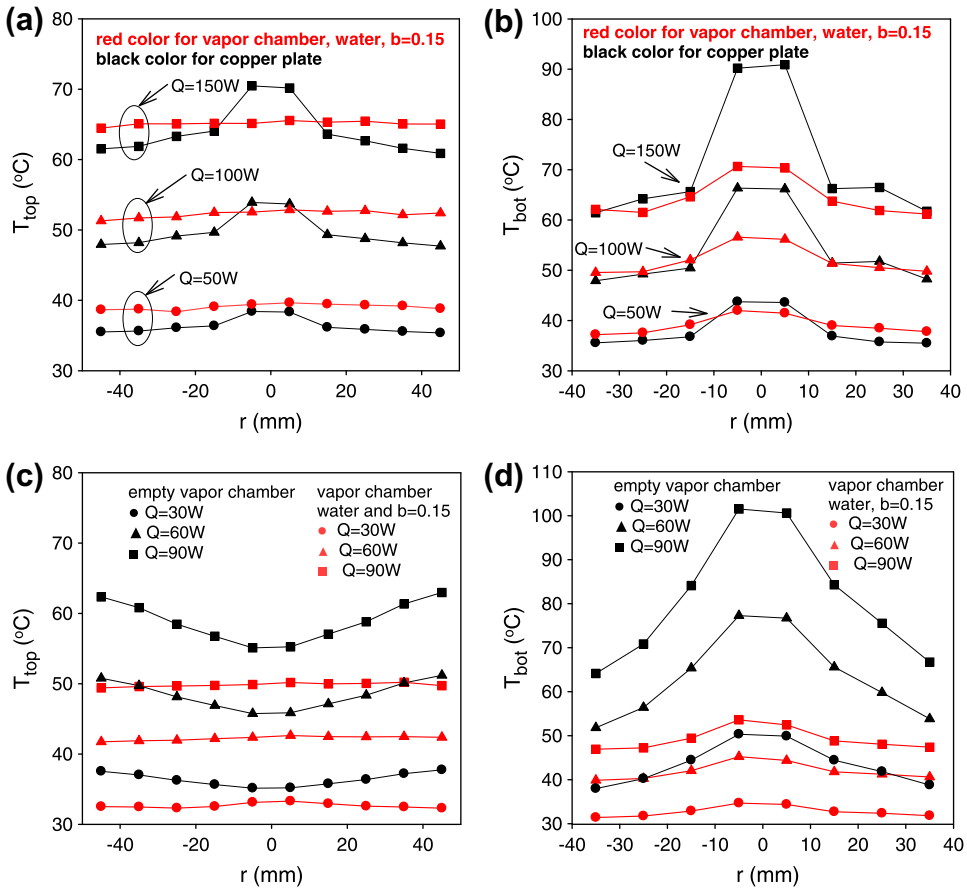

Fig. 6. Temperatures at the top and bottom surfaces for copper plate, empty vapor chamber and liquid charged vapor chamber.

the cases tested, the surface temperature non-uniformity on the bottom surface of the vapor chamber are significantly larger than those on the condenser surface, indicating the major contribution of the evaporator resistances to the whole resistances of the vapor chamber.

Fig. 7c gave the surface temperature non-uniformity on the condenser surface of water charged vapor chamber. The smallest charge ratio of 0.15 gave the lowest surface temperature non-uniformity. The high charge ratio may result in the top copper foam piece partially filled by liquid, increasing the surface temperature non-uniformity on the top surface. The situation is changed on the bottom surface of the vapor chamber (see Fig. 7d). The high charge ratio of 0.45 leads to small surface temperature non-uniformity on the bottom surface for $Q < 75$ W. However, when the heating power exceeds 75 W, the moderate charge ratio of 0.30 has the lowest surface temperature non-uniformity. Because the thermal resistances on the bottom surface are several times of the top surface, it is recommended to select the optimal charge ratio based on the performance of the bottom surface.

Fig. 7e–f illustrates the surface temperature non-uniformity versus a set of heating powers and inclination angles, noting that $\theta = 0°$ and 90° represent the horizontal and vertical orientations, respectively. The general trend is that the horizontal ($\theta = 0°$) and slightly inclined angles ($\theta = 30°$) have smaller surface temperature non-uniformity on the top surface of the vapor chamber (see Fig. 7e). The surface temperature non-uniformity are not much different on the bottom surface of the vapor chamber for different inclination angles. The inclination angle of 60° has the smallest surface temperature non-uniformity for $Q < 75$ W, corresponding to $q = 101$ W/cm^2. But the horizontal orientation ($\theta = 0°$) gave the lowest surface temperature non-uniformity for $Q > 75$ W.

3.3. The thermal resistances of the vapor chamber

Effects of working fluids, inclination angles and charge ratio of liquids on the thermal resistances of the vapor chamber were systematically studied here. Fig. 8a shows the thermal resistance versus a set of heating powers and working fluids. The empty vapor chamber and copper plate have constant thermal resistances versus heating powers, which have the thermal resistances of 0.65 K/W and 0.25 K/W, respectively. The ethanol charged vapor chamber at the charge ratio of 0.30 has poor thermal performance, i.e. the thermal resistance is even larger than that for the empty vapor chamber for $Q < 70$ W, possibly due to the delayed phase change heat transfer in the vapor chamber. Water and acetone charged vapor chambers have similar thermal resistances for $Q < 70$ W. However, the water charged vapor chamber has the smallest thermal resistances for $Q > 70$ W. Fig. 8b demonstrates the thermal resistances versus heating powers and inclination angles. At any inclination angles, the water and ethanol based vapor chambers have the smallest and largest thermal resistances, respectively. The water filled vapor chamber has the smallest thermal resistances at the vertical orientation for small heating powers, but has the best thermal performance at the horizontal orientation for large heating powers.

For the water charged vapor chamber, the thermal resistances are smallest with the horizontal orientation at the small charge ratio of 0.15 (see Fig. 9a). The evaporator wick is immersed in liquid,

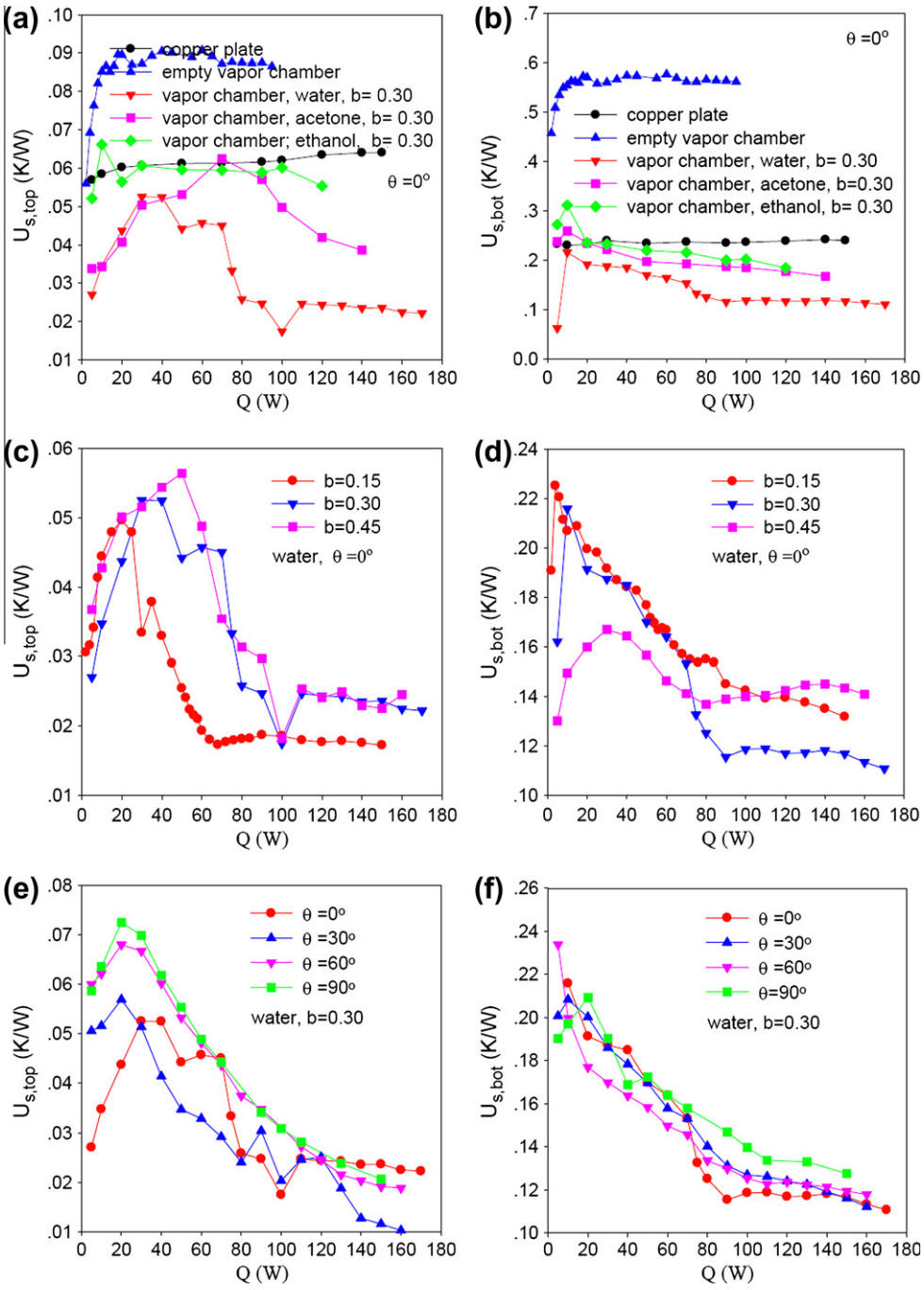

Fig. 7. surface temperature non-uniformity dependent on the working fluid, charge ratio and inclination angle.

while the condenser is filled by vapor. Nucleate boiling is dominated in the evaporator wick while the condenser has low thermal resistance. Increases in the inclination angles decrease the liquid content in the evaporator wick. The differences among different inclination angles become weak at high heat loads, due to the enhanced fluid circulation inside the vapor chamber. When the charge ratio is increased to 0.30, the thermal resistances are smaller for the inclined orientations than that for the horizontal orientation (see Fig. 9b), due to the improved two-phase circulation at low heating loads such as less than 45 W. At high heating loads, the thermal resistances are smallest at the horizontal orientation among the different inclined angles. The charge ratio of 0.45 means nearly half of the vapor chamber internal volume is occupied by liquid, yielding a best thermal performance at the inclination angle of 60° (see Fig. 9c). Both the horizontal and vertical orientations worsen the thermal performance.

3.4. Comparison with other studies

The conclusion on the effect of working fluids on the thermal performance of the vapor chamber is consistent with that drawn by Wong et al. [10]. Here we only compare the thermal resistances of the water charged vapor chamber with those reported in the literature. For most cases tested, the thermal resistances of the vapor chamber are decreased with increases in heating powers. The tested maximum heating power is 170 W at the charge ratio of 0.30 with the horizontal orientation. This corresponds to the heat flux of 216 W/cm^2, at which the minimum thermal resistance is

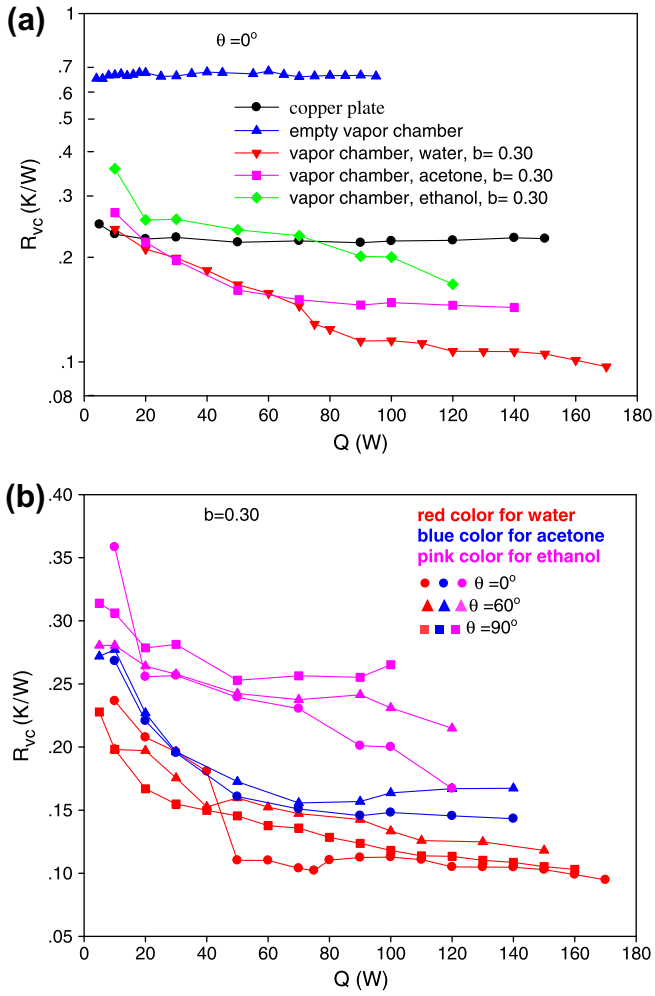

Fig. 8. Thermal resistances of the copper plate, empty vapor chamber and liquid charged vapor chamber for different working fluids and inclination angles.

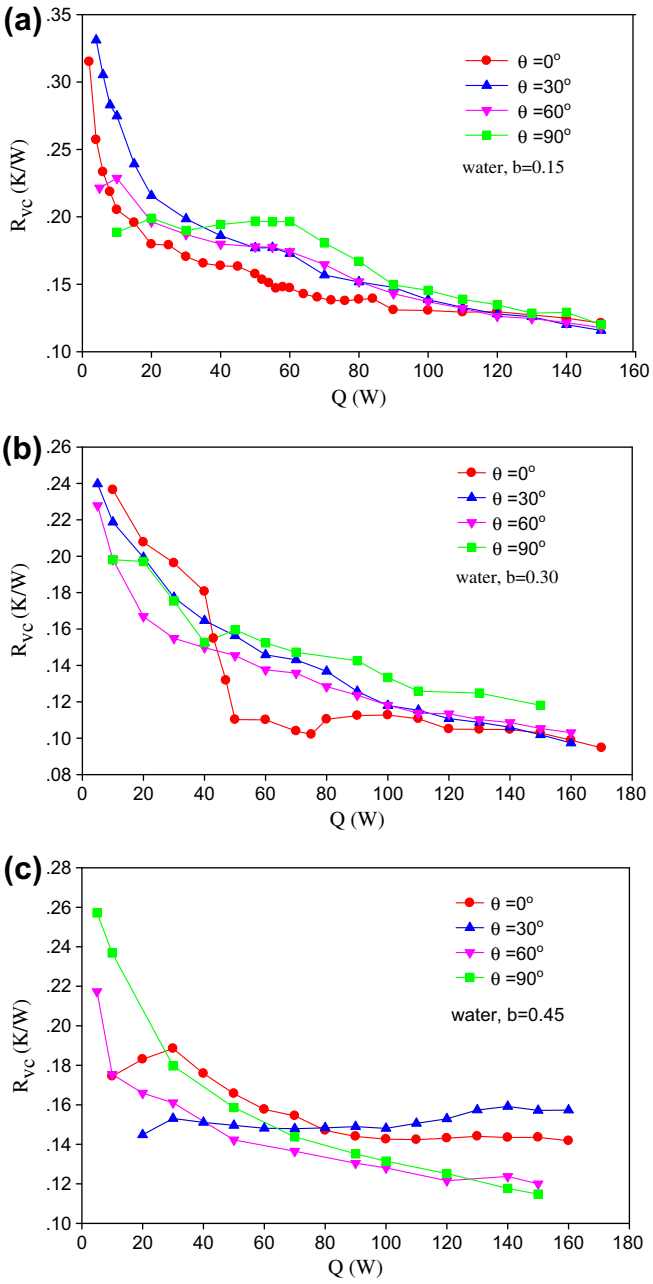

Fig. 9. Effects of inclination angles and charge ratios on the thermal resistance of the vapor chamber.

0.09 K/W (see Fig. 10). Both the capillary limit and the boiling limit are not reached under such circumstance.

Wong et al. [8] studied the performance of a novel vapor chamber, showing smaller liquid flow resistance and hence high anti-dryout capability. Fig. 10 re-plots the thermal resistances versus heat fluxes for the heating area of 1.1 cm by 1.1 cm with water as the working fluid. The charged water has a weight of 3.4 g. The minimum thermal resistance of 0.16 K/W is reached at the heat flux of 124 W/cm^2, which is defined as the transition point, beyond which the thermal resistances are sharply increased, indicating the capillary limit or the boiling limit reached. Wong et al. [10] reported the similar vapor chamber design and tested the thermal performance. As shown in Fig. 10, the curve of thermal resistances versus heat fluxes has a transition point at q = 67 W/cm^2 and R_{VC} = 0.21 K/W, beyond which the thermal resistances will be increased.

Horiuchi [11] developed the vapor chamber using the micro-channel wick instead of the conventional sintered powder wick. They achieved the minimum thermal resistance of 0.17 K/W at the heat flux of 135 W/cm^2, beyond which the thermal performance of the vapor chamber becomes worse.

Chen et al. [12] developed a vapor chamber using the diamond–copper composition as the wick structure. There are three types of diamond–copper powder volume ratio as 1/4, 1/6 and 1/8 considered in fabrication of the wick sheets and columns. They stated that the wick material of diamond–copper composition can effectively prevent the shortcoming of dry-out at high heat flux. As shown in Fig. 10, the tested heat fluxes are less than 57 W/cm^2, covering a narrow range. The thermal resistances begin to rise when the heat flux exceeds 38 W/cm^2 for one type of wick with the diamond to copper powder volume ratio of 1/6.

From the above comparison, it is seen that the copper foam based vapor chamber significantly extends the range of heat fluxes (~220 W/cm^2) without the capillary limit or the boiling limit occurred. The minimum thermal resistance can reach 0.09 K/W. Such high heat flux dissipation using vapor chambers was less reported in the literature, to the authors' knowledge. The significantly extended heat flux range is based on the following mechanisms.

3.5. The high porosity

The copper foam has a high porosity of 0.95, which is larger than the porosity of 0.3–0.6 for conventional porous media. The

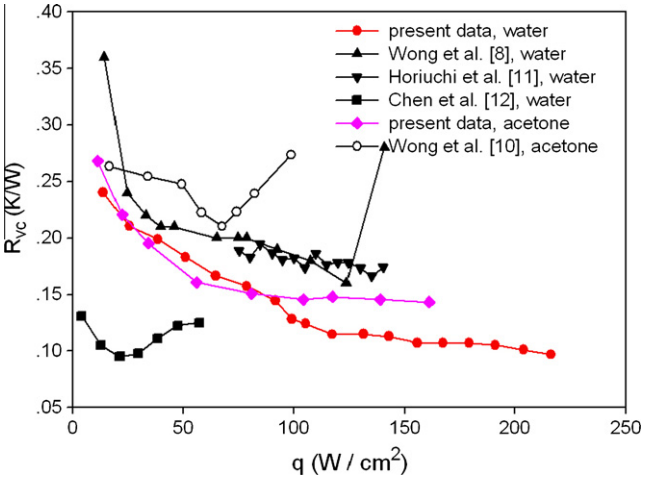

Fig. 10. Comparisons of thermal resistances among the present study and those reported in the literature.

high porosity ensures a larger foam thickness used and decreases the flow resistance of the two-phase circulation in the vapor chamber. Besides, the copper foam vapor chamber provides significantly larger extended heat transfer area than the microchannel based vapor chamber.

3.6. The multiscale pore size

Due to the distinct nature of the metallic foam, multiscale pore sizes existed. The larger pores help to release the created vapor while the smaller pores help to suck the liquid toward the heater surface, decreasing the shear stress at the vapor–liquid interface for the counter-current flow.

3.7. The shortcut of the flow path

The copper foam bars directly contact the tip of the top and bottom copper foam pieces to significantly decrease the liquid flow path from the condenser surface to the evaporator wick.

4. Conclusions

We presented the experimental study on the vapor chamber performance using copper foam as the capillary wick. The conclusions are summarized as follows.

(1) The theoretical analysis on the working principle of the vapor chamber using porous media as the wick structure yields two parameters. One refers to the geometry structure for the wick, the other is the N parameter, relating to the physical properties of working fluids. Water and ethanol have the largest and smallest N numbers, among the three working fluids of water, acetone and ethanol.

(2) Except the thermal resistances defined in the literature, the surface thermal resistance is newly defined to characterize the temperature uniformity on the evaporator and condenser surfaces. The surface temperature non-uniformity on the bottom evaporator surface are several times of those on the top condenser surface.

(3) For most cases, the surface temperature non-uniformity on the evaporator and condenser surfaces display parabola shape, i.e. they will be increased, attain the maximum value and then decreased with continuously increases in heating loads. Generally, the working fluid of water, horizontal orientation, and charge ratio of 0.30 gave the lowest surface temperature non-uniformity.

(4) At the small charge ratio of 0.15, thermal resistances of the vapor chamber are smallest with the horizontal orientation. For the moderate charge ratio of 0.30, the inclined or vertical orientations improve the thermal performance at low heating powers, but the horizontal orientation has the lower thermal resistances for large heating powers. Inclined or vertical orientations have smaller thermal resistances at the high charge ratio of 0.45.

(5) The maximum heating power of 170 W corresponds to the heat flux of 216 W/cm^2, with the minimum thermal resistance of 0.09 K/W, under which the capillary limit or boiling limit is not reached. The significantly extended heat flux range is due to the distinct nature of high porosity and multiscale pore sizes of copper foams.

Acknowledgements

This work was supported by the Joint Fund of the National Natural Science Foundation of China and Guangdong Province (U1034004), Natural Science Foundation of China for distinguished young scholars (50825603), and the National Basic Research Program of China (2011CB710703).

References

[1] Y. Wang, K. Vafai, Transient characterization of flat plate heat pipes during startup and shutdown operations, Int. J. Heat Mass Transfer 43 (2000) 2641–2655.
[2] Y. Wang, K. Vafai, An experimental investigation of the thermal performance of an asymmetrical flat plate heat pipe, Int. J. Heat Mass Transfer 43 (2000) 2657–2668.
[3] Y.X. Wang, G.P. Peterson, Investigation of a novel flat heat pipe, J. Heat Transfer ASME 127 (2005) 165–170.
[4] Y. Cao, M. Gao, Experiments and analyses of flat miniature heat pipes, energy conversion engineering conference, in: IECEC 96 Proceedings of the 31st Inter Society, 1996.
[5] R. Hophins, A. Faghri, D. Khrustalev, Flat miniature heat pipe with micro capillary grooves, J. Heat Transfer Trans. ASME 121 (1999) 02–109.
[6] L.L. Vasiliev, Micro and miniature heat pipes-electronic component coolers, Appl. Therm. Eng. 28 (2008) 266–273.
[7] M.H. Lu, L. Mok, R.J. Bezama, A graphite foams based vapor chamber for chip heat spreading, J. Electron. Pack. 128 (2006) 427–431.
[8] S.C. Wong, K.C. Hsieh, J.D. Wu, W.L. Han, A novel vapor chamber and its performance, Int. J. Heat Mass Transfer 53 (2010) 2377–2384.
[9] V.V. Calmidi, Transport phenomenon in high porosity metal foams, PhD thesis, University of Colorado, CO, 1998.
[10] S.C. Wong, S.F. Huang, K.C. Hsieh, Performance tests on a novel vapor chamber, Appl. Therm. Eng. 31 (2011) 1757–1762.
[11] Y. Horiuchi, M. Mochizuki, K. Mashiko, Y. Saito, Micro Channel Vapor Chamber for high heat Spreading, in: 10th Electronics Packaging Technology Conference, 2008, pp. 749–754.
[12] Y.T. Chen, J.M. Miao, D.Y. Ning, T.F. Chu, W.E. Chen, Thermal performance of a vapor chamber heat pipe with diamond–copper composition wick structures, Int. Microsyst. Pack. Assembly Circ. Technol. Conf. (2009) 340–343.